Multi-objective Design Optimization of Branching, Multifloor, Counterflow Microheat Exchangers

Abas Abdoli
Department of Mechanical
and Materials Engineering,
Florida International University,
MAIDROC Laboratory, EC2960,
10555 West Flagler Street, EC3462,
Miami, FL 33174
e-mail: aabdo004@fiu.edu

George S. Dulikravich
Professor and Director of MAIDROC
Fellow ASME
Department of Mechanical
and Materials Engineering,
Florida International University,
MAIDROC Laboratory, EC2960,
10555 West Flagler Street, EC3462,
Miami, FL 33174
e-mail: dulikrav@fiu.edu

Heat removal capacity, coolant pumping power requirement, and surface temperature nonuniformity are three major challenges facing single-phase flow microchannel compact heat exchangers. In this paper multi-objective optimization has been performed to increase heat removal capacity, and decrease pumping power and temperature nonuniformity in complex networks of microchannels. Three-dimensional (3D) four-floor configurations of counterflow branching networks of microchannels were optimized to increase heat removal capacity from surrounding silicon substrate ($15 \times 15 \times 2$ mm). Each floor has four different branching subnetworks with opposite flow direction with respect to the next one. Each branching subnetwork has four inlets and one outlet. Branching patterns of each of these subnetworks could be different from the others. Quasi-3D conjugate heat transfer analysis has been performed by developing a software package which uses quasi-1D thermofluid analysis and a 3D steady heat conduction analysis. These two solvers were coupled through their common boundaries representing surfaces of the cooling microchannels. Using quasi-3D conjugate analysis was found to require one order of magnitude less computing time than a fully 3D conjugate heat transfer analysis while offering comparable accuracy for these types of application. The analysis package is capable of generating 3D branching networks with random topologies. Multi-objective optimization using modeFRONTIER software was performed using response surface approximation and genetic algorithm. Diameters and branching pattern of each subnetwork and coolant flow direction on each floor were design variables of multi-objective optimization. Maximizing heat removal capacity, while minimizing coolant pumping power requirement and temperature nonuniformity on the hot surface, were three simultaneous objectives of the optimization. Pareto-optimal solutions demonstrate that thermal loads of up to 500 W/cm^2 can be managed with four-floor microchannel cooling networks. A fully 3D thermofluid analysis was performed for one of the optimal designs to confirm the accuracy of results obtained by the quasi-3D simulation package used in this paper.
[DOI: 10.1115/1.4027911]

Keywords: electronics cooling, microheat exchanger, multi-objective optimization, conjugate heat transfer, single-phase flow microchannel

1 Introduction

Cooling systems for new generation portable electronic devices with higher capacity of heat removal, higher efficiency and smaller size is one of the challenges in the heat transfer field. The heat dissipation of microprocessors has delineated an exponential increase over the past decade and up to 10 times larger heat fluxes, with respect to current devices, are expected in next-generation microelectronics [1].

One of the cooling system technologies is the cooling microchannel based compact heat sink. Significantly smaller sizes of the microchannels offer major advantage of this method which allows multichip integration. The main challenges of this method are high pressure drop which require higher pumping power, surface temperature nonuniformity, liquid maldistribution, and coolant leaks [2]. Microchannel heat sinks have been investigated both experimentally and numerically [1–6]. Single-phase flow heat transfer in microchannels has been studied by many investigators.

Heat transfer coefficients and friction factors in microchannels have been experimentally investigated by Kosar and Peles [7] for heat fluxes ranging from 3.8 to 167 W/cm^2. Colgan et al. [8] investigated practical implementation of a single-phase microchannel flow in silicon substrates to enhance removal of heat load up to 300 W/cm^2 using water as coolant. Walchli et al. [9] applied oscillating flow method on water cooling system for thin form factor high performance electronics with 180 W/cm^2 heat flux load.

A computational and experimental investigation of pressure losses and heat transfer in microchannel networks containing T-type junctions have been performed by Haller et al. [10]. Kim et al. [11] numerically studied the thermal and hydraulic performance of single-phase microchannel flows versus phase change flows for different coolants.

One of the first vestiges of the application of optimization methods to improve channel geometries was in the design of gas turbine blades. Martin and Dulikravich [12] presented a fully automated program for inverse design and optimization of cooling passages in internally cooled turbine blades, which was validated against experimental results from Pratt & Whitney Aircraft Company. A few years later, Jelisavcic et al. [13] applied hybrid evolutionary optimization to the same concept of channel network optimization for turbomachinery applications. Hong et al. [14] presented a great effort to enhance the cooling uniformity of microchannel heat exchangers through the design of fractal tree-like networks, attempting to reduce coolant pumping power.

Contributed by the Heat Transfer Division of ASME for publication in the Journal of Heat Transfer. Manuscript received September 14, 2013; final manuscript received June 20, 2014; published online July 15, 2014. Assoc. Editor: Oronzio Manca.

Subsequently, Gonzales et al. [15] executed relevant work comprising 2D microchannel networks optimization. Genetic algorithms have been used by Wei and Joshi [16] to perform single objective optimization in order to minimize overall thermal resistance. Husain and Kim [17] performed single objective optimization using response surface approximation in order to find optimal microchannel width, depth, and fin width.

There is still a need for more research on single-phase flow microchannels in order to increase heat transfer efficiency and decrease temperature nonuniformity and pressure drop [18].

In this paper, a cooling scheme involving 3D networks of branching microchannels is introduced. Results of an optimization study of the topological and geometrical properties of such networks are presented. Topological characteristics include branching pattern and flow direction on each floor with microchannels; geometrical properties include microchannel diameters. This work represents a significant improvement over the initial effort [19] to develop a high efficiency compact heat exchanger based on optimally branched networks of cooling microchannels.

2 Mathematical Model Description

An automatic 3D conjugate heat transfer analysis software package (CHETSOLP) was developed to model conjugate heat transfer phenomena and calculate flow-field and temperature field simultaneously in order to assess any microchannel heat sink topology. The most relevant numerical algorithms comprising the CHETSOLP package are described in this section. The working logic of the package is to solve the flow-field, transfer the flow-field data to the 3D heat conduction analysis code, solve for temperature field in the solid part of the heat exchanger, transfer temperature data to the quasi-1D flow solver via cooling microchannel surfaces, and iteratively repeat this procedure until the wall temperatures of the microchannels (initially guessed) converge. Data transfer at the solid/fluid interfaces is performed by a developed boundary condition transfer module that links the fluid and solid domain solvers. CHETSOLP consist of two parts; random geometry generator and analysis solvers.

3 Random Geometry Generators

A FORTRAN code was written to produce different microchannels arrangements by randomly generating branching patterns, diameters of each branch and direction of each subnetwork on each floor. In the next step, the required stl file for analysis solvers is generated automatically by this code.

In this research, microchannels have been arranged in four floors inside the silicon substrate with dimension of $15 \times 15 \times 2$ mm (length, width, and thickness), as shown in Fig. 1(*a*).

Figure 1(*b*) shows one single floor which has four separate branching subnetworks. Each branching subnetwork has four inlets and one outlet. Branching subnetworks have opposite directions with respect to each other. Total number of branching subnetworks for the four-floor arrangement studied here is 16.

4 Analysis Solvers

In order to perform conjugate heat transfer analysis, two solvers have been coupled to each other; quasi-1D fluid flow and convective heat transfer solver (COOLNET) [12] and 3D heat conduction solver (OpenFOAM) [20].

4.1 Quasi-1D Fluid Flow and Convective Heat Transfer Analysis (COOLNET). The numerical algorithm for integration of mass, momentum, and energy balance equations that follows, assumes steady, incompressible flow, and breaks down each cooling channel into a number of constant cross hydraulic diameter fluid elements [12,19,21].

Mass continuity is enforced throughout by means of solving Eq. (1) at every junction node, that is, at every junction of microchannels the sum of incoming mass flow rates and outgoing mass flow rates must balance out

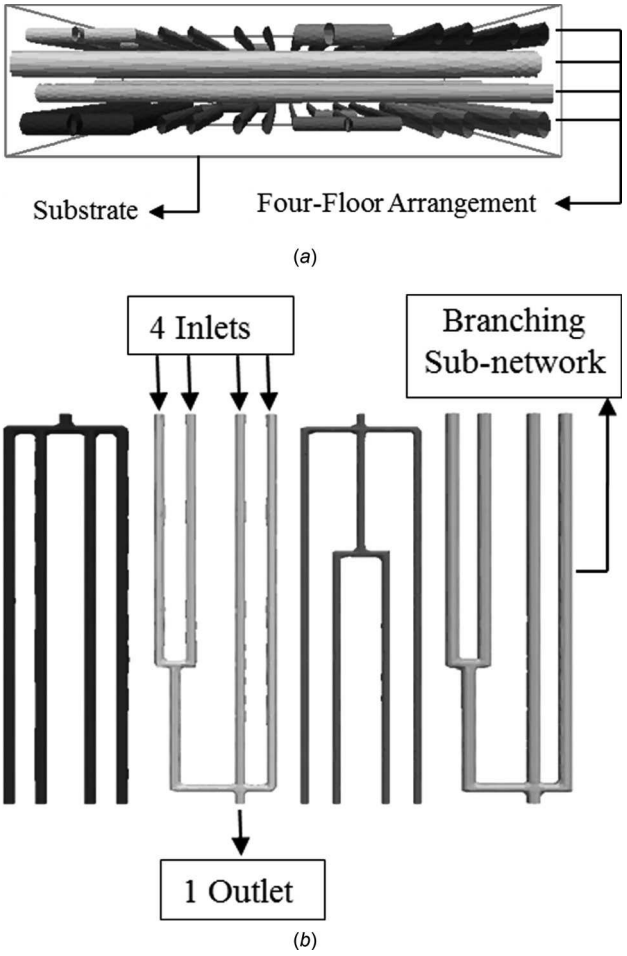

Fig. 1 Microchannel configuration: (*a*) 3D four-floor microchannels and (*b*) four branching subnetworks on one floor

$$\sum_{k=1}^{K\max} \dot{m}_k = \sum_{k=1}^{K\max} \rho V_k A_k = 0 \tag{1}$$

Energy balance equation (First Law of Thermodynamics) for quasi-1D, steady flow results in the extended Bernoulli's equation for the entire channel loop that includes a coolant pump [22], in the case of no work of electromagnetic forces

$$\dot{m}\left[C_{v2}T_2 + \left(\frac{p_2}{\rho_2} + \frac{V_2^2}{2} + gz_2\right)\right] - \dot{m}\left[C_{v1}T_1 + \left(\frac{p_1}{\rho_1} + \frac{V_1^2}{2} + gz_1\right)\right] = \dot{Q} - \left(\dot{W}_{\text{visc}} - \dot{W}_{\text{pump}}\right) \tag{2}$$

At this point, it should be recognized that thermal energy transferred to the fluid by convection has been stored in the fluid as its internal energy, that is

$$\dot{m}(C_{v2}T_2 - C_{v1}T_1) = \dot{Q} \tag{3}$$

After recognizing that potential energy differences are negligible, total pressure loss between the inlet and the outlet of each cooling passage is given as

$$\Delta p_t = \left(p_1 + \rho\frac{V_1^2}{2}\right) - \left(p_2 + \rho\frac{V_2^2}{2}\right) = \frac{\dot{W}_{\text{visc}}}{\dot{m}} \tag{4}$$

since pump is outside the cooling microchannel network in our case (it is in the outer part of the closed-loop cooling system).

The viscous losses are typically grouped into major losses (due to friction of fluid and the channel wall) and minor losses (due to flow separation at locations of inlets, exits, turns, sudden changes of hydraulic diameter, branch nodes/merge nodes of the flow network). Thus

$$\dot{W}_{\text{visc}} = \dot{m}\left(\sum_{i=1}^{\text{Imax}} f_i \frac{L_i}{D_{\text{h}}}\frac{V_i^2}{2} + \sum_{j=1}^{\text{Jmax}} K_j \frac{V_j^2}{2}\right) \tag{5}$$

The Darcy friction factor is calculated for laminar flow conditions as $f = 64/\text{Re}$. For turbulent flow conditions, it is approximated from Eq. (6) as a function of Reynolds number and the relative wall roughness. Equation (6) was proposed by Chen [23]. Ghanbari et al. [24] demonstrated that Chen's equation is one of the most accurate friction factor equations

$$\frac{1}{\sqrt{f}} = -2\log\left\{\frac{\varepsilon/D_{\text{h}}}{3.7065} - \frac{5.0452}{\text{Re}}\log\left[\frac{(\varepsilon/D_{\text{h}})^{1.1098}}{2.8257} + \frac{5.8506}{\text{Re}^{0.8981}}\right]\right\} \tag{6}$$

In the scope of this work, minor losses due to three types of microchannel junctions were addressed: elbows, T-junctions and cross junctions. Inlet losses were also incorporated.

Minor loss coefficients (friction factors), K, of regular-size junctions were used due to lack of data for microsize junctions, especially with circular cross section. Cross junction friction factor recently represented by Sharp et al. [25], was applied in loss calculations. Other minor loss coefficients have been extracted from literature [26–30] so that for inlet/exit $K = 0.5$, for elbow $K = 0.3$, for T-junction $K = 0.2$ and for cross junction $K = 0.16$.

Notice that shaft power (pump power delivered to the fluid) required to push the fluid through the network at a given mass flow rate can be expressed as

$$\dot{W}_{\text{pump}} = -\dot{m}\frac{\Delta p_{\text{t}}}{\rho} + \dot{m}\left(\sum_{i=1}^{\text{Imax}} f_i \frac{L_i}{D_{\text{h}}}\frac{V_i^2}{2} + \sum_{j=1}^{\text{Jmax}} K_j \frac{V_j^2}{2}\right) \tag{7}$$

indicating that pump must overcome the rate of loss of total pressure and viscous losses.

If constant wall temperature is assumed in each constant hydraulic diameter fluid segment of a cooling channel, the rate of heat transferred into the flowing fluid is defined as

$$\dot{Q} = \dot{m}C_v(T_{\text{out}} - T_{\text{in}}) \tag{8}$$

Considering a heating scenario where the channel wall temperature is higher than the fluid temperature, the bulk fluid temperature will rise in the direction of the flow. If a constant cross section fluid element is considered, the energy balance of such differential control volume is given by

$$d\dot{Q} = \dot{m}C_v dT = h(T_{\text{w}} - T)dS \tag{9}$$

which after integration gives the exit fluid bulk temperature that can be computed from Eq. (10), when inlet temperature, wall temperature, heat transfer coefficient, mass flow rate, and fluid's specific heat are known

$$T_{\text{out}} = T_{\text{w}} - (T_{\text{w}} - T_{\text{in}})e^{-\frac{hS}{\dot{m}C_v}} \tag{10}$$

The convective heat transfer coefficient, h, can be calculated from Eq. (11) if Nusselt number is known

$$\text{Nu} = \frac{hD_{\text{h}}}{k} \tag{11}$$

In order to calculate Nusselt number and hence the convective heat transfer coefficient, h, the second Petukhov equation (Eq. (12)) is used [31]. It represents a relationship between the Nusselt, Prandtl, and Reynolds numbers and friction factor for steady, incompressible flow in a straight circular cross section tube.

$$\text{Nu} = \frac{(f/8)(R_e - 1000)P_r}{1 + 12.7(f/8)^{0.5}(P_r^{2/3} - 1)} \tag{12}$$

Based on Eq. (7), for $\dot{W}_{\text{pump}} = 0$ and $\Delta p_{\text{t}} = \text{constant}$, viscous losses will be constant. In such cases, having a larger velocity and a smaller friction factor may seem to be desirable because it increases the mass flow rate and, as a result of it, the convection heat transfer will increase according to Eq. (3). On the other hand, based on Eq. (10), increasing the velocity (or mass flow rate) leads to a smaller fluid exit temperature. This decreases the temperature difference between inlet and outlet, and based on Eq. (3), it decreases the convection heat transfer. Finding optimal mass flow rate in a manner that maximizes the heat transfer while minimizing the rate of viscous losses will be addressed in this study.

The quasi-1D thermofluid solver (COOLNET) is an iterative scheme that decouples continuity and momentum from energy balance. It was formulated, developed and tested by Martin and Dulikravich [12,19,21]. The definition of the momentum conservation matrix system is straightforward for every channel. The mass conservation matrix balance is expressed on a nodal basis rather than on a channel-by-channel basis. Therefore, the formulation of such matrix system is entirely dependent on the branching pattern that a given node exhibits.

The quasi-1D thermofluid analysis code COOLNET is capable of automatically assembling such matrix system involving mass, momentum, and energy balance equations based on the microchannels' connectivity. The matrix system is composed of a coefficient matrix, a vector of unknowns and a boundary conditions vector. The coefficients matrix is composed in a specific form depending on channels' connectivity. This matrix of coefficients multiplies the unknown vectors which are assembled by placing: (1) the equivalent total pressures for all internal nodes, that is, all channel junctions except for the inlet and outlet ports and (2) average channel mass flow rates. The boundary conditions vector stores quantities derived from prescribed values at the domain boundaries. Complex network topologies yield slightly ill-conditioned matrices. Therefore, singular value decomposition algorithm [19,21] was used for matrix inversion at all iterations. A matrix inversion subroutine solves for equivalent total pressures and mass flow rates simultaneously. For the 3D temperature field solution in the substrate material, no matrix system is required. A simple advancing-front program (OpenFOAM platform [20]) sweeps the microchannel network solving Eq. (5) for all nodes (except for inlets). Wall temperatures, calculated mass flow rate, channel lengths and cross-sectional areas are considered for solution of this equation.

Jelisavcic et al. [13] investigated the COOLNET solver in terms of accuracy and speed against an analytical solution yielded by the Hagen–Poiseuille equation, and also against a high-fidelity 3D Navier–Stokes equations solver (ANSYS CFX). They reported less than 8% error for the large Re numbers against analytical solution. They also demonstrated that ANSYS CFX has more accuracy compared to the COOLNET, but that it also requires approximately 50 times more computing time as compared to COOLNET. This confirms the large economical advantage of using quasi-3D conjugate thermofluid analysis models instead of using complete 3D Navier–Stokes equations with turbulence modeling.

4.2 3D Heat Conduction Analysis. Steady 3D heat conduction analysis inside the heat exchanger solid material was carried out with commercial software OpenFOAM [20] which uses the Gaussian finite volume (hexahedral cells) integration method for

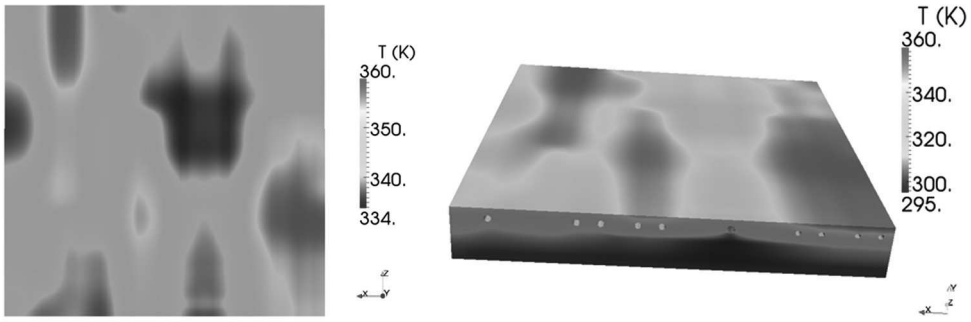

Fig. 2 Temperature distribution for a nonoptimized configuration: (*a*) hot surface (having large temperature variations CV = 1.711×10^{-2}) and (*b*) entire 3D substrate

computation of derivatives and it implements a linear interpolation scheme. The accuracy of OpenFOAM solver was discussed by Dulikravich and Martin [21]. They demonstrated that for a 2D test case, the OpenFOAM LaPlace solver has very good accuracy with maximum error less than 1% against analytical solution.

5 Test Case Definition

For the purpose of demonstrating the utility of the developed design optimization algorithm for 3D networks of cooling channels, we simulated a silicon substrate that has a footprint of 15 mm by 15 mm and a thickness of 2 mm with thermal conductivity $k = 130\,\mathrm{W\,m^{-1}\,K^{-1}}$. A uniform thermal load of $500\,\mathrm{W/cm^2}$ was enforced on the top surface of the substrate and a constant temperature of 300 K was enforced at the bottom surface of the substrate. A dielectric liquid coolant was simulated as pumped at horizontal floors each containing four branching subnetworks to absorb as much heat as possible. Manufacturing limitations suggested by Jones et al. [32] constrain microchannel hydraulic diameters to be greater than 100 μm and relative wall roughness to be not less than 7% of the hydraulic diameter. The most relevant characteristics are

(1) maximum number of planar branching levels: 2,
(2) minimum hydraulic diameter: 200 μm, and
(3) maximum hydraulic diameter: 350 μm.

In this work, the interior wall relative roughness was kept constant at 7% for all the branches in the cooling networks since optimizing variation of surface roughness was shown [19] to be potentially detrimental in multi-objective optimization. Different investigators have reported different critical Reynolds numbers for fluid flows inside microchannels [33]. In most research, laminar flows were observed for Reynolds number less than 2000. Therefore, in this research, critical Reynolds number has been set at 2000. The boundary conditions for water coolant at the inlet were: total pressure of 270 kPa and total temperature of 293 K. The boundary condition at the exits was the static pressure of 110 kPa. Fluid properties are temperature-dependent and were imported from OpenFOAM's fluid database [20]. The local average coolant velocities, pressures and temperatures were then calculated by iteratively satisfying a system of local mass conservations and extended Bernoulli's equations [12,19,21,22].

5.1 A Random Unoptimized Configuration. Conjugate heat transfer in an initial population of 1341 unique randomly generated four-floor branching microchannel networks was simulated using CHETSOLP. Results of one of these cases are shown in this section.

Coefficient of variation (CV) was defined as the ratio of standard deviation (σ) over the average value (T_{ave}) of temperature on the hot surface, where N is the number of cells on the surface, that is

$$\mathrm{CV} = \frac{\sigma}{T_{\mathrm{ave}}}, \quad \sigma = \sqrt{\frac{1}{N}\sum_{i=1}^{N}(T_i - T_{\mathrm{ave}})^2}, \quad T_{\mathrm{ave}} = \frac{1}{N}\sum_{i=1}^{N} T_i \tag{13}$$

Figure 2(*a*) shows the temperature distribution on the hot surface, while Fig. 2(*b*) shows the 3D temperature distribution in the entire substrate. This figure demonstrates that the large variations in temperature field occur close to the hot surface.

Wall temperature distributions on all floors are shown in Fig. 3(*a*). Figures 3(*b*)–3(*e*) show temperature distribution on each microchannel floor. The first floor temperature variation is illustrated in Fig. 3(*b*). This floor is next to the cold surface.

As these figures show, temperature field in each floor is affected by temperature fields on its top and bottom floors. On the fourth floor which is the closet floor to the hot surface (Fig. 3(*e*)), in some branching subnetworks, higher temperatures are observed at the beginning of channels. This happens because Reynolds numbers in those channels are less than critical Reynolds number which is 2000 for microchannels with 7% relative surface roughness [33]. By merging channels, since the diameter in a given subnetwork is constant, the Reynolds number will be increased and as a result of this, the convection heat transfer coefficient, h, and the amount of heat removed will be increased. Therefore, lower temperatures of the channel walls will be seen at the end of subnetworks of microchannels.

Calculated mass flow rate, heat removal, viscous losses and diameter of each branching subnetwork are presented in Table 1. Viscous losses in this table were calculated from Eq. (5). Mass flow rate is varying by the diameter and branching pattern. As results show, branching subnetwork #14 performs the maximum amount of heat removal.

Table 2 illustrates the mass flow rate, heat removed, and viscous losses (Eq. (5)) for each floor. Floor #4, which is the closest floor to the hot surface, has the maximum amount of heat removal, minimum mass flow rate and minimum pumping power requirement.

6 Multi-objective Optimization

Optimization of the topology and geometrical characteristics of the 3D microchannel network was performed by using modeFRONTIER software [34]. In this paper, design variables for a single branching subnetwork include three variables for branching pattern and one for diameter. There are three more design variables for directions of floors. Therefore, for 16 branching subnetworks, the total number of design variables is 67. The 67 design variables which are defining the four-floor cooling configuration of microchannel networks were randomly varied to generate 1341 unique four-floor cooling topologies. Then, these 1341 unique

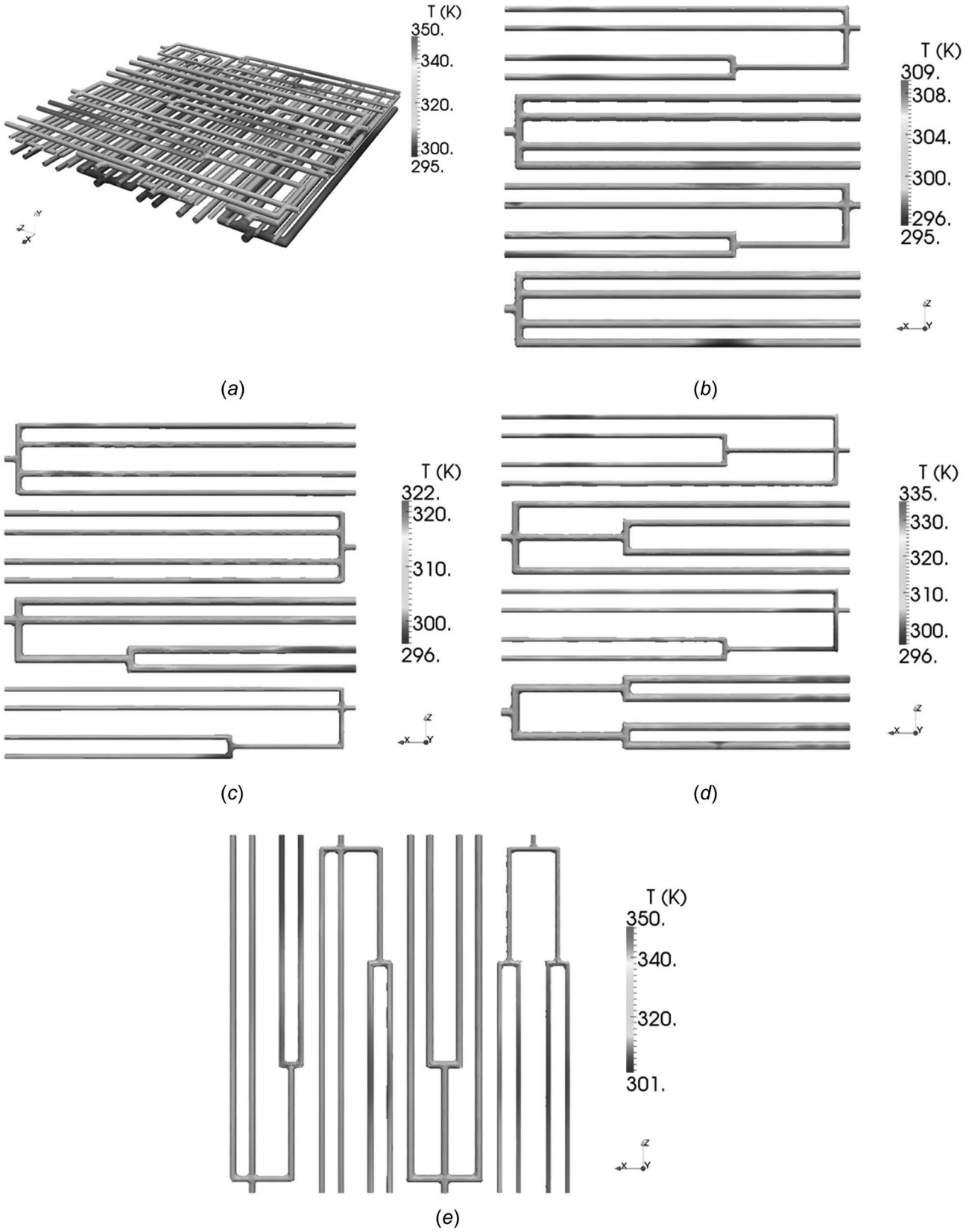

Fig. 3 Temperature distribution for nonoptimized microchannel walls: (*a*) four-floor microchannels, (*b*) first floor, (*c*) second floor, (*d*) third floor, and (*e*) fourth floor

Table 1 Analysis results for all branching subnetworks in non-optimized case

Branching subnetwork	Mass flow rate (g/s)	Heat removed (W)	Viscous losses Eq. (5) (W)	Microchannel diameter (μm)
1	3.34	54.787	0.539	250
2	2.03	20.709	0.328	250
3	3.34	46.838	0.539	300
4	1.23	13.235	0.198	200
5	0.77	4.747	0.124	200
6	3.08	61.499	0.497	300
7	1.39	30.733	0.247	200
8	1.39	45.697	0.247	350
9	2.63	97.457	0.425	250
10	0.77	11.408	0.124	250
11	2.05	76.583	0.331	350
12	0.74	6.707	0.122	200
13	0.57	37.466	0.092	250
14	2.05	119.638	0.331	350
15	1.23	49.385	0.198	300
16	1.23	87.925	0.198	350

Table 2 Analysis of results for all floors in nonoptimized case

Floor No.	Mass flow rate (g/s)	Heat removed (W)	Viscous losses Eq. (5) (W)
1	9.93	135.569	1.605
2	6.63	142.675	1.114
3	6.19	192.155	1.001
4	5.07	294.414	0.819
Total	27.80	764.814	4.539

random cases were imported to modeFRONTIER to generate the 67-dimensional response surface which is a powerful method to interpolate multivariate scattered data and decrease cost of computations. Response surface methodology was implemented using Gaussian radial basis function (GRBF).

Multi-objective Genetic Algorithm II (NSGA-II) was chosen to perform optimization. NSGA-II is a multi-objective evolutionary algorithm developed by Deb et al. [35,36]. The three simultaneous objectives of the optimization study were:

(1) maximize total heat removed,
(2) minimize pumping power due to major and minor losses, and
(3) minimize temperature nonuniformity on hot surface.

The main difficulty was to create an accurate response surface for a large number of integer design variables, (67 variables) which was capable to predict the three objectives with an acceptable error. GRBF based response surface offered more accurate results in comparison to other response surface methods. A GRBF was created by using 1341 unique randomly generated four-floor cooling networks. Then, this GRBF was coupled to NSGA-II multi-objective optimization algorithm in modeFRONTIER software in order to perform the optimization. The Pareto front obtained by this method is illustrated in Fig. 4 by two objectives; pumping power and total heat removal. These Pareto designs are shown by green squares and named "Virtual Pareto." Blue circles represent the 1341 random initial cases and named "Initial Population."

In the next step, 25 different virtual Pareto designs obtained by modeFRONTIER optimization were chosen as input data for 3D CHETSOLP. The analysis results are shown by red squares and named "Real Pareto" in Fig. 4. As this figure shows, in the region between 800 W and 900 W of thermal power removed, which has more initial points, the virtual and real Pareto designs are well matched. The differences between virtual and real Pareto designs are higher at the head and tail of initial population cloud. This is

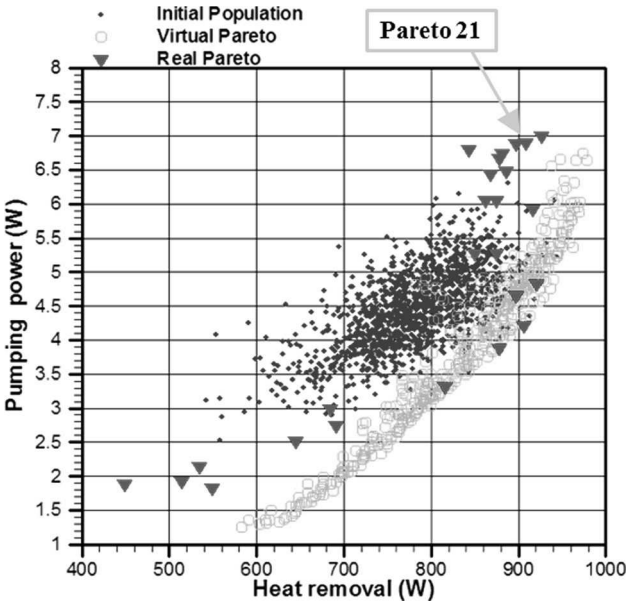

Fig. 4 Thermal energy removed versus pumping power requirement for initial population, virtual Pareto, and real Pareto-optimal designs

because the GRBF does not have enough points in these regions to predict the behavior of objectives with respect to variables. However, the real Pareto still represents good dominant designs in comparison with initial population.

Figure 5 shows initial population, virtual Pareto and real Pareto for CV with respect to total heat removed. As this figure illustrates, virtual and real Pareto designs are in good agreement in almost all regions.

One of the best real Pareto optimized designs (Pareto No. 21) was chosen to be studied more by using its analysis results. Pareto No. 21 results are shown in Figs. 6 and 7.

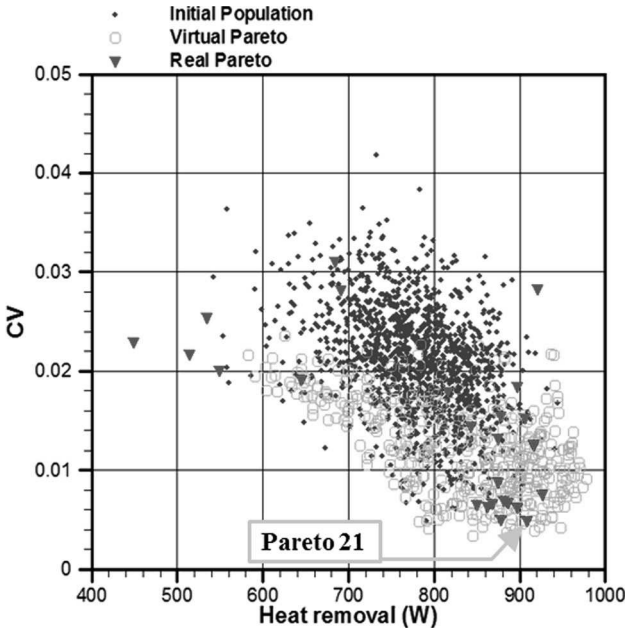

Fig. 5 CV versus total heat removed for initial population, virtual Pareto designs, and real Pareto designs

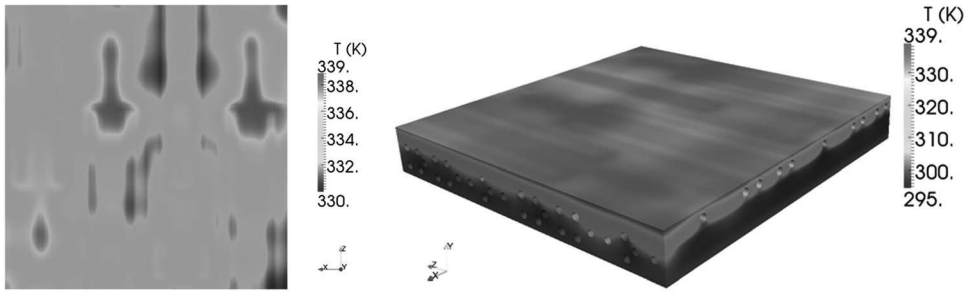

Fig. 6 Temperature distribution for Pareto optimized cooling network No. 21 when using quasi-3D conjugate analysis: (*a*) hot surface and (*b*) 3D substrate

Figures 6(*a*) and 6(*b*) demonstrate the temperature distribution on the hot surface and substrates, respectively. Temperature on the hot surface is changing from 330 K to 339 K. A significant drop in the maximum temperature and temperature nonuniformity is observed in this case. The CV on the hot surface for this case was 4.907×10^{-3}.

Temperature distributions on all four floors are shown in Figs. 7(*a*)–7(*e*). Figure 7(*e*) shows a quite uniform temperature distribution on the top floor.

Table 3 shows mass flow rate, heat removed, viscous losses (from Eq. (5)) and diameter of each branching subnetworks. Subnetwork #14 had the maximum heat removal. The minimum mass flow rate and minimum viscous losses were obtained for branching subnetworks #5 and #11, respectively.

Results represented in Table 4 indicate that the fourth floor (top floor) removes 4.15 times more heat than the first floor.

6.1 Measures of Cooling Efficiency. The measure of cooling efficiency of this convection cooling scheme can be expressed in several ways and it strongly depends on using the minimum possible amount of pumping power which is provided by batteries in the case of portable electronics. In certain publications [15,37], pumping power is defined based on the total pressure loss only, while not including the viscous losses from Eq. (7). Such idealized coefficient of efficiency of a cooling scheme uses ratio of total amount of heat removed by coolant divided with the idealized pumping power [15,37]

$$\eta_{\text{visc}} = \frac{\dot{Q}_{\text{conv}}}{\dot{m}\Delta p_{\text{t}}/\rho} \tag{14}$$

Another very useful measure of the efficiency of the cooling scheme is the percentage of the heat load that was removed by the coolant

$$\eta_{\text{conv}} = \frac{\dot{Q}_{\text{conv}}}{\dot{Q}_{\text{load}}} \tag{15}$$

In applications where this cooling concept is used in portable systems, an appropriate measure of efficiency should include the sum of the power expended on making the electric circuitry operate and generate the heat load and the power needed to compensate for power consumed by inviscid and viscous forces (Eq. (7)). Thus, such ultimate measure of efficiency should be

$$\eta_{\text{total}} = \frac{\dot{Q}_{\text{conv}}}{\dot{Q}_{\text{load}} + \dot{W}_{\text{visc}}} \tag{16}$$

The optimal design may require more power for pumping the coolant, but at the same time, it has a much higher heat removal capacity. Table 5 shows various measures of efficiency, standard deviation of temperature, and CV for the random nonoptimized cooling network which was studied in Sec. 5.1 and for Pareto optimized configuration No. 21.

By comparing the results, it is apparent that Pareto optimized configuration No. 21 gives higher uniformity in temperature distribution on the hot surface. These results also illustrate that Pareto optimized configuration No. 21 has 34% higher pumping power than the random design. However, the total amount of heat removed over the heat load achieved by the Pareto design No. 21 is 13% higher than in the case of a random nonoptimized design.

7 Fully 3D Thermofluid Conjugate Analysis

In this section, a fully 3D conjugate thermofluid analysis was performed to study the accuracy of CHETSOLP package which performs only quasi-1D thermofluid analysis coupled with a fully 3D heat conduction analysis. Multiregion heat transfer solver (chtMultiRegionSimpleFoam) of OpenFOAM was used for steady state simulation. Reynolds-averaged Navier–Stokes equations were applied with the k-ε turbulence model.

The total numbers of grid cells in each branching subnetwork and in substrate were 158,062 and 3,199,690, respectively.

Figure 8(*a*) shows the temperature distribution on the hot surface of substrate in the case of Pareto #21 optimized design when using fully 3D conjugate analysis. This temperature distribution is in good agreement with CHETSOLP (quasi-3D) conjugate analysis shown in Fig. 6(*a*). Hot spots predicted by the CHETSOLP simulation are in the same locations and of the same magnitude as those obtained by fully 3D simulation.

Table 6 demonstrates the maximum temperature and temperature nonuniformity on the hot surface obtained by both methods. The maximum temperature obtained by CHETSOLP is 2 K less than maximum temperature obtained by fully 3D conjugate heat transfer simulation (using 3D Navier–Stokes equations). The temperature nonuniformity calculated by CHETSOLP is slightly higher than the one obtained by fully 3D simulation.

Convergence history for temperature field inside substrate is shown in Fig. 9. As this figure shows, CHETSOLP quasi-3D conjugate analysis was converged after 200 iterations and fully 3D conjugate analysis after 400 iterations.

However, average CHETSOLP run required around 900 s, while fully 3D conjugate analysis required 10,800 s for the same level of convergence. Simulations were performed on a machine with 16 GB RAM and Intel® Core™ i7-3770 CPU @ 3.40 GHz × 8 processor.

8 Conclusions

Single-phase 3D microchannels with four-floor configurations have been investigated using the CHETSOLP package which applies quasi-1D fluid flow and convective heat transfer solver (COOLNET) and 3D heat conduction solver (OpenFOAM). Each

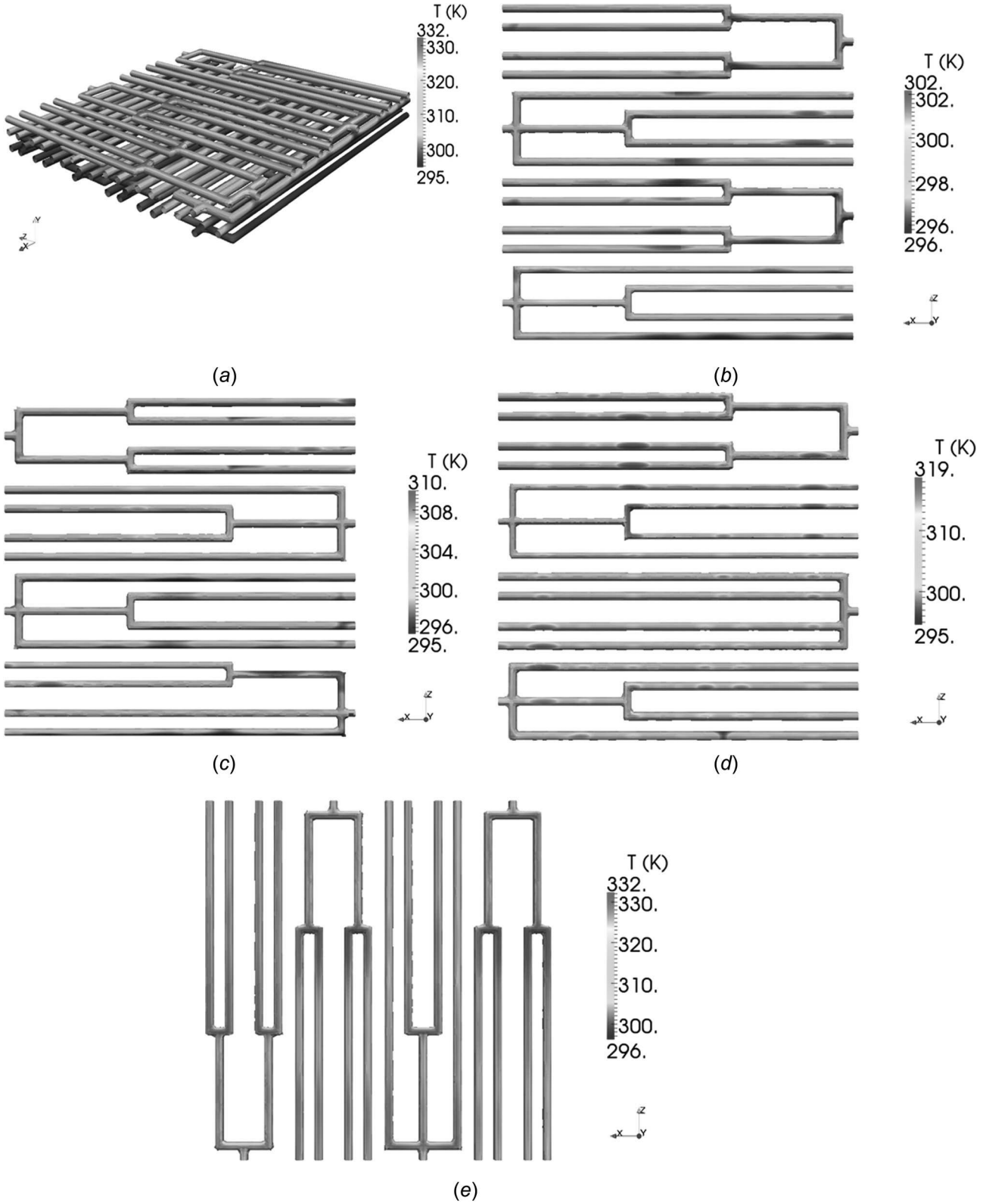

Fig. 7 Temperature distribution on (*a*) four-floor microchannels, (*b*) first floor, (*c*) second floor, (*d*) third floor, and (*e*) fourth floor of the Pareto optimized cooling network No. 21

floor had four branching subnetworks. The analysis results for random unoptimized microchannels have been discussed.

Multi-objective optimization was performed using mode-FRONTIER software. Branching pattern and diameter of each branching subnetwork, and flow direction of each floor were design variables for optimization. Total number of design variables for 16 subnetworks was 67 integers. Maximizing amount of heat removed, minimizing temperature nonuniformity on hot surface, and minimizing viscous losses were three objectives of this optimization problem. GRBF response surface and genetic algorithm (NSGA-II) have been chosen to perform optimization. Among different response surface methods, GRBF gives better

Table 3 Analysis results for all branching subnetworks for Pareto optimized case No. 21

Branching subnetwork No.	Mass flow rate (g/s)	Heat removed (W)	Viscous losses Eq. (5) (W)	Microchannel diameter (μm)
1	2.046	26.292	0.331	300
2	2.632	24.076	0.425	350
3	3.12	31.281	0.504	350
4	2.632	24.717	0.425	350
5	2.03	20.590	0.328	300
6	3.12	33.002	0.504	350
7	3.12	41.599	0.504	350
8	2.632	31.497	0.425	350
9	3.12	74.189	0.504	350
10	3.336	65.151	0.539	350
11	1.252	38.043	0.202	250
12	2.632	55.609	0.425	350
13	2.632	109.575	0.425	350
14	3.12	122.913	0.504	350
15	2.632	104.246	0.425	350
16	2.632	105.231	0.425	350

Table 4 Analysis results for all four floors for Pareto optimized configuration No. 21

Floor	Mass flow rate (g/s)	Heat removed (W)	Viscous losses Eq. (5) (W)
1	10.43	106.370	1.690
2	10.90	126.690	1.760
3	10.34	232.990	1.670
4	11.02	441.960	1.780
Total	42.69	908.01	6.90

Table 5 Cooling efficiency measures, standard deviation of hot surface temperature, and CV for the random design and Pareto optimized configuration No. 21

Case	η_{visc}	η_{conv} (%)	η_{total} (%)	σ (K)	CV
Random Case	168.498	67.984	68.782	5.910	1.71×10^{-2}
Pareto #21	131.596	80.712	81.932	1.640	4.91×10^{-3}

results for a large number of design variables. Results of 1341 unique random cases obtained from CHETSOLP were used to create a GRBF.

Twenty-five of virtual Pareto-optimal designs obtained from modeFRONTIER were then analyzed using CHETSOLP. The simulation results of these 25 designs (real Pareto) have shown good agreement with virtual Pareto-optimal designs and have represented good dominant designs in comparison to initial population. Results of one of the real Pareto-optimal configurations (No. 21) have shown a significant improvement in temperature uniformity. The percentage of the removed heat by microchannels over the heat load (η_{conv}) for this design is 80.72%, which is about 13% higher than in the case of the random nonoptimized design.

Table 6 Comparison of CHETSOLP (quasi-3D conjugate) and fully 3D conjugate heat transfer analysis results for Pareto-optimal design No. 21

Conjugate analysis	T (K)	σ (K)	CV
Quasi-3D	339	1.640	4.91×10^{-3}
Fully 3D	341	1.086	3.21×10^{-3}

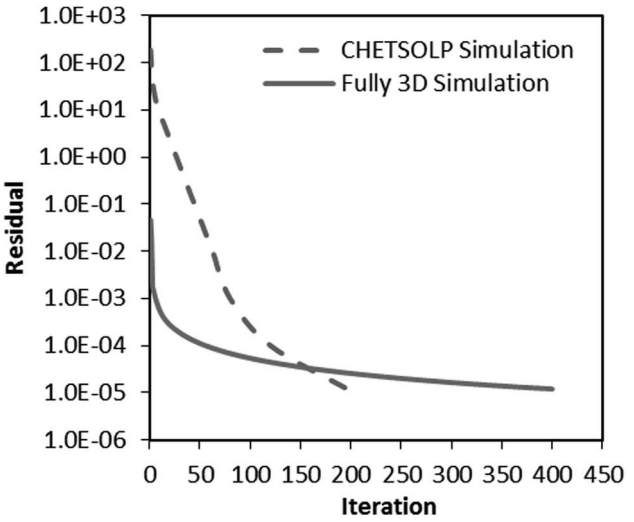

Fig. 9 Convergence histories for temperature field inside the substrate obtained using two conjugate analysis codes

A fully 3D conjugate analysis was then performed for Pareto-optimal solution No. 21 to investigate the accuracy of the CHETSOLP package. The CHETSOLP results were in good agreement with fully 3D simulation results, while offering one order of magnitude reduction in computing time. This paper shows that approximately 80% of the imposed heat flux will be removed by convection if four floors of optimized branching microchannels are used. If more floors are used, it is to be expected that higher percentage of the imposed heat flux can be removed by convection at the expense of the increased viscous losses. The remaining amount of heat will have to be removed by cooling the bottom surface (say, with a fan). An alternative boundary condition on the bottom surface could have been (especially in the case when total thickness of the microheat exchanger is limited so adding more

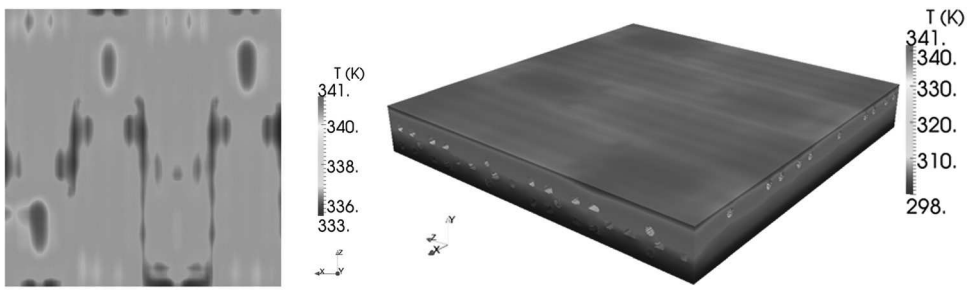

Fig. 8 Temperature distribution for Pareto optimized design No. 21 when using fully 3D conjugate analysis: (*a*) hot surface and (*b*) 3D substrate

floors is not an option) to impose a realistic convection heat transfer coefficient and ambient fluid temperature there. In this case, minimization of temperature of the bottom surface should be performed as an additional objective function.

Acknowledgment

Authors would like to express their gratitude to Professor Carlo Poloni, founder and president of ESTECO, for providing modeFRONTIER software free of charge for this project.

Nomenclature

A = cross-sectional area of a microchannel
CV = hot surface temperature nonuniformity
C_v = specific heat per unit mass at constant volume
D_h = hydraulic diameter
f = Darcy friction factor for pipe flow
g = gravity acceleration
h = convection heat transfer coefficient
k = thermal conductivity of the fluid
K = coefficient of minor viscous losses
L = length of the cooling channel
$\dot{m}$ = mass flow rate
Nu = Nusselt number
p = static pressure
Pr = Prandtl number
$\dot{Q}$ = total heat transferred into fluid
Re = Reynolds number
S = surface area of the microchannel
T = absolute temperature
T_{ave} = average temperature
v = velocity vector magnitude
$\dot{W}_{pump}$ = pump power transmitted to the coolant
$\dot{W}_{visc}$ = power consumed by viscous losses
z = elevation of a point
Δp_t = total pressure loss

Greek Symbols

ε = channel inner wall surface roughness
η_{conv} = ratio of heat removed by coolant over thermal load
η_{tot} = ratio of heat removed by coolant over sum of thermal load and viscous losses
η_{visc} = ratio of heat removed by coolant over power consumed by viscous losses
ρ = density
σ = standard deviation of hot surface temperature

Subscripts

in = microchannel inlet
out = microchannel exit/outlet
w = microchannel wall

References

[1] Mudawar, I., 2001, "Assessment of High-Heat-Flux Thermal Management Schemes," IEEE Trans. Compon. Packag. Technol., **24**(2), pp. 122–141.
[2] Ebadian, M. A., and Lin, C. X., 2011, "A Review of High-Heat-Flux Heat Removal Technologies," ASME J. Heat Transfer, **133**(11), p. 110801.
[3] Pence, D. V., 2000, "Improved Thermal Efficiency and Temperature Uniformity Using Fractal Tree-Like Branching Channel Networks," *Heat Transfer and Transport Phenomena*, G. P. Celata, V. P. Carey, M. Groll, I. Tanasawa, and G. Zummo (eds.), Begell House, New York. pp. 142–148.
[4] Bowers, M. B., and Mudawar, I., 1994, "High Flux Boiling in Low Flow Rate, Low Pressure Drop Mini-Channel and Micro-Channel Heat Sinks," Int. J. Heat Mass Transfer, **37**(2), pp. 321–332.
[5] Kim, S. J., and Kim, D., 1999, "Forced Convection Cooling in Microstructures for Electronic Equipment Cooling," ASME J. Heat Transfer, **121**(3), pp. 639–645.
[6] Fedorov, A. G., and Viskanta, R., 2000, "Three-Dimensional Conjugate Heat Transfer in the Microchannel Heat Sink for Electronic Packaging," Int. J. Heat Mass Transfer, **43**(3), pp. 399–415.
[7] Kosar, A., and Peles, Y., 2006, "Thermal-Hydraulic Performance of MEMS-Based Pin Fin Heat Sink," ASME J. Heat Transfer, **128**(2), pp. 121–131.
[8] Colgan, E. G., Furman, B., Gaynes, M., Graham, W., LaBianca, N., Polastre, R. J., Rothwell, M. B., Bezama, R. J., Choudhary, R., Marston, K., Toy, H., Wakil, J., Zitz, J. A., and Schmidt, R., 2007, "A Practical Implementation of Silicon Microchannel Coolers for High Power Chips," IEEE Trans. Compon. Packag. Technol., **30**(2), pp. 218–225.
[9] Walchli, R., Brunschwiler, T., Michel, B., and Poulikakos, D., 2010, "Self-Contained, Oscillating Flow Liquid Cooling System for Thin Form Factor High Performance Electronics," ASME J. Heat Transfer, **132**(5), pp. 1–9.
[10] Haller, D., Woias, P., and Kockmann, N., 2009, "Simulation and Experimental Investigation of Pressure Loss and Heat Transfer in Microchannel Networks Containing Bends and T-Junctions," Int. J. Heat Mass Transfer, **52**(11–12), pp. 2678–2689.
[11] Kim, Y. J., Joshi, Y. K., Fedorov, A. G., Lee, Y.-J., and Lim, S.-K., 2010, "Thermal Characterization of Interlayer Microfluidic Cooling of Three-Dimensional Integrated Circuits With Nonuniform Heat Flux," ASME J. Heat Transfer, **132**(4), pp. 1–9.
[12] Martin, T. J., and Dulikravich, G. S., 2001, "Aero-Thermo-Elastic Concurrent Design Optimization of Internally Cooled Turbine Blades," *Coupled Field Problems* (Series on Advances in Boundary Elements, A. J. Kassab, and M. H. Aliabadi, eds., WIT Press, Boston, MA, pp. 137–184.
[13] Jelisavcic, N., Martin, T. J., Moral, R. J., Sahoo, D., Dulikravich, G. S., and Gonzalez, M., 2005, "Design Optimization of Networks of Cooling Passages," ASME Paper No. IMECE2005-79175.
[14] Hong, F. J., Cheng, P., Ge, H., and Joo, T., 2006, "Design of a Fractal Tree-Like Microchannel Net Heat Sink for Microelectronic Cooling Limerick, Ireland," Paper No. ICNMM2006-96157.
[15] Gonzales, M. J., Jelisavcic, N., Moral, R. J., Sahoo, D., Dulikravich, G. S., and Martin, T. J., 2007, "Multi-Objective Design Optimization of Topology and Performance of Branching Networks of Cooling Passages," Int. J. Therm. Sci., **46**(11), pp. 1191–1202.
[16] Wei, X., and Joshi, Y., 2002, "Optimization Study of Stacked Micro-Channel Heat Sinks for Micro-Electronic Cooling," Proceedings of the ITherm 2002, San Diego, CA, June 1, pp. 441–448.
[17] Husain, A., and Kim, K.-Y., 2009, "Thermal Optimization of a Microchannel Heat Sink With Trapezoidal Cross Section," ASME J. Electron. Packag., **131**(2), pp. 1–6.
[18] Kandlikar, S. G., 2010, "Microchannels: Rapid Growth of a Nascent Technology," ASME J. Heat Transfer, **132**(4), pp. 1–2.
[19] Martin, T. J., and Dulikravich, G. S., 2002, "Analysis and Multi-Disciplinary Optimization of Internal Coolant Networks in Turbine Blades," AIAA J. Propul. Power, **18**(4), pp. 896–906.
[20] OpenCFD Ltd., "OpenFOAM., 2000–2013," http://www.opencfd.co.uk/openfoam/
[21] Dulikravich, G. S., and Martin, T. J., 2010, "Optimization of 3D Branching Networks of Micro-Channels for Microelectronic Device Cooling," 14th International Heat Transfer Conference—IHTC, Washington, DC, Aug. 7–13, Paper No. IHTC14-22719.
[22] Cengel, Y. A., and Cimbala, J. M., 2010, *Fluid Mechanics: Fundamentals and Applications*, 2nd ed., McGraw-Hill, New York, p. 373.
[23] Chen, N. H., 1979, "An Explicit Equation for Friction Factor in Pipe," Ind. Eng. Chem. Fundam., **18**(3), pp. 296–297.
[24] Ghanbari, A., Farshad, F. F., and Rieke, H. H., 2011, "Newly Developed Friction Factor Correlation for Pipe Flow and Flow Assurance," J. Chem. Eng. Mater. Sci., **2**(6), pp. 83–86.
[25] Sharp, Z. B., Johnson, M. C., Barfuss, S. L., and Rahmeyer, W. J., 2010, "Energy Losses in Cross Junctions," J. Hydraul. Eng., **136**(1), pp. 50–55.
[26] White, F. M., 2008, *Fluid Mechanics*, 6th ed., McGraw-Hill, New York.
[27] Streeter, V. L., and Wylie, E. B., 1985, *Fluid Mechanics*, 8th ed., McGraw-Hill, New York.
[28] Hamilton, J. B., 1929, "University of Washington Engineering Experimental Station Bulletin," p. 51.
[29] Harris, C. W., 1928, "University of Washington Engineering Experimental Station Bulletin," p. 48.
[30] Hydraulic Institute, 1979, *Engineering Data Book*, 1st ed., Cleveland Hydraulic Institute, Cleveland, OH.
[31] Abdoli, A., and Dulikravich, G. S., 2013, "Optimized Multi-Floor Throughflow Micro Heat Exchangers," Int. J. Therm. Sci., **78**, pp. 111–123.
[32] Jones, K. W., Liu, Y.-Q., and Cao, M.-C., 2003, "Micro Heat Pipes in Low Temperature Cofire Ceramic (LTCC) Substrates," IEEE Trans. Compon. Packag. Technol., **26**(1), pp. 110–115.
[33] Saha, A. A., and Mitra, S. K., 2012, *Microfluidics and Nanofluidics Handbook: Chemistry, Physics, and Life Science Principles*, Taylor & Francis Group, Boca Raton, FL, pp. 139–155.
[34] "modeFRONTIER Optimization Software," http://www.esteco.com
[35] Deb, K., Pratap, A., Agarwal, S., and Meyarivan, T., 2000, "A Fast and Elitist Multi-Objective Genetic Algorithm-NSGA-II," KanGAL Report No. 2000001.
[36] Deb, K., and Agrawal, R. B., 1995, "Simulated Binary Crossover for Continuous Search Space," Complex Syst., **9**(2), pp. 115–148.
[37] Bejan, A., 2000, *Shape and Structure, From Engineering to Nature*, Cambridge University, Cambridge, UK.